

## Structural Rearrangements in 5,10,15,20-Tetrakis(4-sulfonatophenyl)porphyrin J-Aggregates under Strongly Acidic Conditions

Maria Angela Castriciano,<sup>†</sup> Andrea Romeo,<sup>†,‡</sup> Valentina Villari,<sup>§</sup> Norberto Micali,<sup>§</sup> and Luigi Monsù Scolaro<sup>\*,†,‡</sup>

*Dipartimento di Chimica Inorganica, Chimica Analitica e Chimica Fisica, Università di Messina, Salita Sperone 31, 98166 Vill.S.Agata, Messina, Italy, INFN, Unità di Messina, Messina, Italy, and CNR-Istituto per i Processi Chimico-Fisici, sez. Messina, Via La Farina 237, 98123, Messina, Italy*

*Received: November 5, 2002; In Final Form: May 30, 2003*

Recently, we showed that J-aggregates, formed by the zwitterionic diacid form of the porphyrin 5,10,15,20-tetrakis(4-sulfonatophenyl)porphyrin ( $H_2TPPS_4^{4-}$ ) under acidic conditions, can be described in terms of fractal geometry. We have extended the investigation of the system under strongly acidic conditions through a combination of UV/vis and fluorescence emission spectroscopy, together with static (SLS), quasi-elastic (QELS), and resonant (RLS) light-scattering techniques. The experimental findings suggest that porphyrin J-aggregates begin to form at pH 1 and are stable up to 4 M HCl. On further increasing the acid concentration, protonation of the sulfonate end groups occurs, leading to a disruption of the electrostatic interactions between these anionic groups and the charged protonated nitrogen atoms in the porphyrin core. At  $[HCl] > 8$  M, the spectroscopic features suggest the presence of the monomeric dicationic porphyrin, resulting from a full protonation of the four sulfonate groups. Under the acid concentration range in which J-aggregates exist, light-scattering data indicate the formation of clusters having a fractal internal structure. At  $[HCl] = 0.1$  M, the aggregation is driven by the interaction between small clusters leading to a loose diffusion-limited cluster–cluster aggregation (DLCCA) structure ( $d_f = 1.75 \pm 0.05$ ). On increasing the acid concentration up to 2 M HCl, a structural crossover occurs. The reduction of the net charge on the monomeric unit leads to an increased sticking probability between monomers which is responsible for the observed compact diffusion-limited aggregation (DLA) structure ( $d_f = 2.5 \pm 0.03$ ). A further reduction of the net charge of the porphyrin ( $[HCl] = 4$  M) determines the formation of nucleating clusters no longer having a fractal structure. An important role is played by the mixing order of the reagents both at the level of kinetics of growth and for the final mesoscopic structures. Our findings suggest that this effect should be related to the large volumetric ratio between the reagent solutions to be mixed, which causes very different spatial concentrations of both reagents.

### Introduction

Aggregation of small molecules to form organized arrays of chromophores is a subject of topical interest due to the many implications in different fields of supramolecular sciences.<sup>1</sup> Usually these assemblies exhibit peculiar physicochemical properties (well distinct from the isolated monomer), important from a fundamental point of view and suitable for possible technological applications, e.g., materials with enhanced non-linear optical susceptibilities.<sup>2</sup> In this respect, J-aggregates are common for different classes of aromatic compounds, e.g., cyanine dyes.<sup>3,4</sup> In the case of J-aggregates derived from cyanine dyes, relevant applications as photographic sensitizers<sup>5</sup> have been developed due to their giant absorption cross section and exciton delocalization capability.<sup>6,7</sup>

Recently, the porphyrin 5,10,15,20-tetrakis(4-sulfonatophenyl)porphyrin ( $H_2TPPS_4^{4-}$ ) has attracted the interest of various researchers because its diacid form ( $H_4TPPS_4^{2-}$ ), under acidic conditions (usually  $pH < 1$ ), forms J-aggregates.<sup>8–17</sup> Formation of these J-aggregates can be induced also by different cationic species (alkaline-earth metal ions, monoamines,<sup>12</sup> surfactants<sup>18</sup>

and cationic porphyrins<sup>19,20</sup>). These species exhibit an intense and narrow bathochromically shifted absorption band at 490 nm, which has been assigned to a Frenkel exciton-like transition.<sup>21</sup> The sharpness of this band with respect to the monomer has been interpreted in terms of motional narrowing, which averages the local inhomogeneities.<sup>22</sup> In the present case, the  $\sigma$ – $\pi$  stacking interactions, which are usually invoked to explain the occurrence of attraction between adjacent porphyrin rings,<sup>23–25</sup> are overcome by an interplay of electrostatic and hydrogen-bonding interactions acting between the anionic sulfonate groups, on the phenyl *meso*-substituents, and the positively charged protonated nitrogen atoms in the porphyrin core.

A series of investigations showed that a large number of porphyrins are involved in single aggregates,<sup>14,15</sup> whose average size is in the order of hundreds of nanometers. Light-scattering experiments have pointed out that these aggregates are organized in the mesoscopic scale forming self-similar or fractal structures in the  $\mu m$  range, which behave as colloidal systems.<sup>16</sup>

In a fractal aggregate, a scaling law of the form  $M \sim R^{d_f}$  relates the mass of the cluster,  $M$ , to its radius  $R$ , where  $d_f$  is the fractal dimension ( $d_f < 3$  and not an integer number). This exponent is not only a structural parameter, being connected to the density of the clusters, but it is also a signature of the mechanism of aggregation. Statistical physics and computer simulations have related its value to different growth pro-

\* Corresponding author. Telephone: +39 090 6765711. Fax: +39 090 393756. E-mail: monsu@chem.unime.it.

<sup>†</sup> Università di Messina.

<sup>‡</sup> INFN, Unità di Messina.

<sup>§</sup> CNR-Istituto per i Processi Chimico-Fisici.

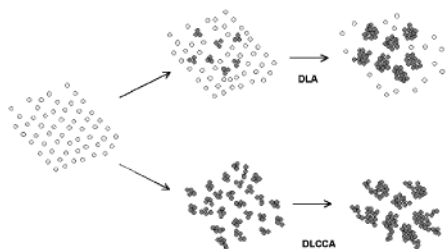


**Figure 1.** Models for the growth of fractal aggregates through an initial slow RLA mechanism followed by DLA or DLCCA faster mechanisms.

cesses: (i) percolation and diffusion-limited aggregation (DLA),  $d_f = 2.5$ ; (ii) diffusion-limited cluster-cluster aggregation (DLCCA),  $d_f = 1.75$ ; (iii) reaction limited aggregation (RLA),  $d_f = 2.1$ .<sup>26</sup> Diffusion-limited aggregation mechanisms differ in the sticking probability of the monomers and small clusters in solutions. The time evolution of the aggregation process can be described by the Smoluchowski rate equation:

$$C_j + C_m \xrightarrow{K(j,m)} C_{j+m}$$

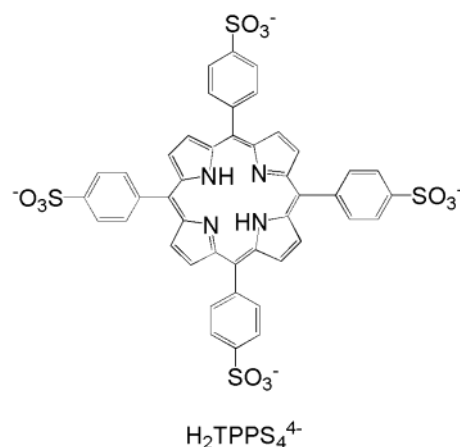
which relates the disappearance rate of the species  $j$  and  $m$  to form species  $j+m$ .  $C_j$  denotes an aggregate containing  $j$  monomers and  $K(j,m)$  is the reaction kernel, which for self-similar objects fulfils the conditions  $K(\lambda j, \lambda m) = \lambda^\lambda K(j,m)$  and  $K(j,1) \approx j^\nu$ , with  $\lambda \leq 1$  and  $\nu \leq 1$ ,<sup>27,28</sup> both related to the fractal dimension. The occurrence of different kinetic processes depends on the quantity  $\mu = \lambda - \nu$ . The DLA regime ( $\lambda < \nu$ ) is dictated by a higher sticking probability between monomers and small clusters, while the DLCCA regime ( $\lambda > \nu$ ) is dominated by the higher sticking probability between small-medium clusters. Both mechanisms, schematically depicted in Figure 1, should be preceded by a reaction limited mechanism, in which a sort of activation barrier has to be reached to make the collision between monomers effective.

In our previous studies, we have shown that other porphyrin systems are able to form fractal aggregates whose structure is strongly controlled by the properties of the solvent medium and by the chemical nature of the building blocks.<sup>20,29–34</sup> In particular, detailed kinetic and structural investigations on the salt-induced aggregation of the 5,15-bis(*N*-methylpyridinium-4-yl)diphenylporphyrin (*trans*-H<sub>2</sub>P<sub>agg</sub>) have evidenced, in agreement with theoretical and experimental studies on model systems, the presence of an early activated process for the formation of initial nuclei in solutions (RLA), which afterward start to interact preferentially with monomers leading to compact DLA type clusters.<sup>32</sup> Anyway, the system undergoes large structural changes depending on the ionic strength and is very sensitive to different initial conditions.<sup>34</sup>

In the case of H<sub>4</sub>TPPS<sub>4</sub><sup>2-</sup> J-aggregates the mesoscopic structure grows with a fast DLCCA mechanism when the aggregation is fostered at pH  $\sim 1$ .<sup>16</sup> Alternatively, under milder acidic conditions, an increase of the ionic strength, by the addition of sodium chloride, drives the systems to RLA type objects, pointing out a different efficiency of H<sup>+</sup> and Na<sup>+</sup> in controlling the final structure. Recently, the formation of such species has been postulated as a relevant step for the chiral induction in stirred solutions of aggregating H<sub>4</sub>TPPS<sub>4</sub><sup>2-</sup>.<sup>35,36</sup>

Here we report an investigation on the stability of acid-induced J-aggregates through a combination of UV/vis, fluorescence emission spectroscopy, and elastic, dynamic, and resonance light scattering. All these techniques are noninvasive and are able to report detailed structural and dynamical information on aggregated species in solution. On increasing

**CHART 1**



the acid concentration from 0.1 to 12 M HCl, we have found that (i) J-aggregates are stable up to 4 M HCl, even if structural rearrangements occur and that, (ii) at concentrations of hydrochloric acid higher than 6 M, the experimental evidences confirm the disruption of the clusters and the formation of fully protonated monomeric species. Furthermore, because of the occurrence of nucleation phenomena, quite common in colloidal systems, we have also investigated the aggregation behavior of this porphyrin by changing the order of adding reagents in solution. Our results suggest a dramatic influence of the mixing order due to largely different spatial concentrations of both reagents under the two adopted protocols.

## Experimental Section

**Materials.** The porphyrin 5,10,15,20-tetrakis(4-sulfonatophenyl)porphyrin (H<sub>2</sub>TPPS<sub>4</sub><sup>4-</sup>, Chart 1) was purchased from Aldrich Co. as the tetrasodium salt. The purity of the porphyrin was checked by the method of Buchler et al.<sup>37</sup> Aqueous stock solutions of this porphyrin were prepared in dust-free Millipore water, stored in the dark, and used within a day of preparation. The concentration of the porphyrin ( $3 \times 10^{-6}$  M) was determined spectrophotometrically using  $\epsilon_{412} = 5.33 \times 10^5$  M<sup>-1</sup> cm<sup>-1</sup> at the Soret maximum in water.<sup>9</sup>

The investigated range of acid concentration (0.1–12 M) was obtained by mixing the porphyrin with a proper amount of concentrated HCl, up to the required final concentration. Because the structure of the resulting aggregates is strongly affected by the mixing order of the reagents (*vide infra*), aggregated porphyrin samples were prepared by two well distinct protocols: (i) addition of the proper amount of concentrated HCl to a diluted porphyrin solution (*porphyrin-first mixing*, PF) and (ii) addition of a stock solution of concentrated porphyrin to a solution containing the acid at the required concentration (*porphyrin-last mixing*, PL).

**Methods.** UV/vis spectra were taken on a Hewlett-Packard model 8453 diode array spectrophotometer using 1 cm path length quartz cells. Fluorescence emission and resonance light-scattering (RLS) experiments were performed on a Jasco mod. FP-750 spectrofluorimeter. In this latter case, a synchronous scan protocol with a right angle geometry has been adopted.<sup>38,39</sup> When dealing with highly scattering samples, neutral density filters were placed in the excitation path (optical density 0.8). Both the emission and resonance light-scattering spectra were not corrected for the absorption of the samples.

Static light scattering (SLS) measurements were performed by using a computerized homemade goniometer and the exciting light source was a 20 mW polarized Nd:YAG laser (532 nm).

The investigated scattering angle range was  $20^\circ \leq \theta \leq 150^\circ$  corresponding to exchanged wave vector values  $5.5 \leq k \leq 30.5 \mu\text{m}^{-1}$  (being the exchanged wave vector  $k = [(4\pi n)/\lambda]\sin(\theta/2)$ , where  $n$  is the refractive index of the sample and  $\lambda$  the vacuum incident wavelength). The measured scattered intensity of the solutions were normalized by the scattered intensity of toluene used as reference. For some acid concentrations small-angle light scattering (SALS) was also performed. The experimental setup for small-angle light scattering (SALS) has been described in a previous paper.<sup>40</sup> This optical apparatus performs an optical Fourier transform of the impinging (scattered) wave front at a linear position sensitive detector. In this case the exciting light source is a 10 mW HeNe laser (632.8 nm,  $0.8 < k < 2.7 \mu\text{m}^{-1}$ ). A fibered 1024 element diode array was used as detector and a 16 bit analog-to-digital converter was employed to digitalize the signal. The intensity scattered by the optical cell filled by the solvent was taken as the background and subtracted from all the measured spectra. Furthermore, data coming from SALS were scaled by a multiplicative factor in order to perform the fitting procedure in all the investigated  $k$  range.

The same experimental setup adopted for SLS experiments was also used to perform quasi-elastic light-scattering (QELS) measurements. The scattered light was collected, in a self-beating mode, through an optical fiber matched with a digital Hamamatsu R942 photomultiplier cooled at  $-30^\circ\text{C}$ . The signal was sent to a Malvern 4700 submicrometer particle analyzer system (eight parallel correlators at different sampling times) and the intensity–intensity correlation function  $g^2(\tau)$  was measured in the time range  $10 \mu\text{s} \leq \tau \leq 1\text{s}$ , using an typical acquisition time of 200 s. Artifacts due to fluorescence have been eliminated by setting an interference filter on the observation path during the SLS and QELS measurements. The investigated samples (2 mL) were placed in a Burchard cylindrical quartz cell (Hellma) and thermostated by a home-made water-circulating system. The temperature controller provided a constant value of 298 K with an accuracy of 0.01 K. The light-scattering experiments were repeated on at least five different samples to check for reproducibility and the results were consistent within the experimental error.

**Data Analysis.** The information on the structural and conformational properties of molecules in solution can be determined by SLS through the measurement of the scattered intensity profile,

$$I(k) \propto P(k)S(k) \quad (1)$$

( $P(k)$  and  $S(k)$  being the form and the structure factor, respectively).<sup>41</sup> Depending on the aggregate size and on the exchanged wave vector values  $k$ , the intensity  $I(k)$  assumes different profiles. From a general point of view, the Guinier law

$$I(k) \propto \exp[-(1/3)(kR_g)^2] \quad (2)$$

is obeyed at low  $k$  values ( $R_g$  being the gyration radius),<sup>41</sup> whereas the Porod limit

$$I(k) \propto k^{-4} \quad (3)$$

is followed at high  $k$  values for which  $kl \gg 1$  ( $l$  being the building blocks size). At intermediate  $k$  values, for which  $kR_g \gg 1$  and  $kl \ll 1$ , the  $k$  dependence of the scattered intensity is dictated by the peculiar structural features of the system, and it can be described according to different models. For large aggregates, for example, the correlation length,  $\xi$ , of the internal

density fluctuations can be described by the Ornstein–Zernike form:<sup>42</sup>

$$I(k) \propto (1 + \xi^2 k^2)^{-1} \quad (4)$$

If the spatial correlation density fluctuation is an homogeneous function, the scattering intensity profile obeys a power law

$$S(k) \propto k^{-d_f} \quad (5)$$

where  $d_f$  is the fractal dimension of the aggregate.<sup>43–46</sup> This occurrence is typical of fractally arranged ideal systems. Real fractal systems, however, do not extend to all space scale, but rather they have a finite size and in such a case the power law behavior of the scattering intensity disappears for low  $k$  values, where the Guinier limit begins. Chen and Teixeira<sup>47</sup> proposed a structure factor suitable for describing a finite fractal aggregate encompassing the Gaussian and the fractal behavior of an aggregate of  $m$  monomers

$$S(k) = \frac{m \sin[(d_f - 1)\arctan(kR)]}{(d_f - 1)kR(k^2 R^2)^{d_f/2 - 1/2}} \quad (6)$$

where  $R$  is the radius of the aggregate, namely the cutoff parameter of the density correlation function of the fractal.<sup>43,44</sup> It is worth noting that, in the  $kR \gg 1$  regime and for  $R/L$  large enough (typically higher than 50), the previous equation becomes the simple fractal power law in eq 5.

Information on dynamical properties of molecules in solution are obtained complementarily by quasi-elastic light scattering. In particular, the photon correlation spectroscopy (PCS) technique allows for the investigation of the dynamics of aggregates through the measurement of the normalized autocorrelation function  $g_2(k, t)$  of the scattered intensity  $I_S(k, t)$ :<sup>41,48–50</sup>

$$g_2(k, t) = \frac{\langle I_S(k, 0)I_S(k, t) \rangle}{\langle I_S(0) \rangle^2} \quad (7)$$

If the scattered field obeys Gaussian statistics, the following relationship, known as Siegert's relation, can be applied:<sup>41</sup>

$$g_2(k, t) = 1 + \alpha |g_1(k, t)|^2 \quad (8)$$

where  $\alpha$  is a constant which depends on the experimental setup and  $g_1(k, t)$  is the normalized field autocorrelation function.

For diffusing monodisperse spherical objects the intensity correlation function decays exponentially, according to

$$g_2(k, t) = 1 + \alpha \exp(-2\Gamma t) \quad (9)$$

For homogeneous, Euclidean, noninteracting monodisperse spheres, under the fulfillment that  $kR \ll 1$ ,

$$\Gamma = D_C k^2 \quad (10)$$

where  $D_C$  is the collective translation diffusion coefficient, which gives information on the hydrodynamic radius through the Einstein–Stokes relation:

$$R_H = \frac{R_H T}{6\pi\eta D_C} \quad (11)$$

with  $\eta$  the solvent viscosity,  $T$  the temperature, and  $k_B$  the Boltzmann constant.<sup>39</sup>  $R_H$  is the “effective” size, depending on

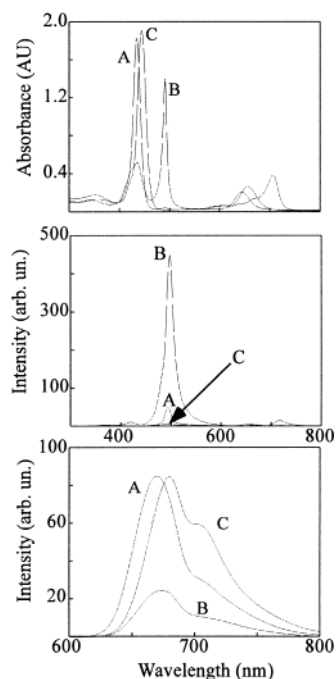


**Figure 2.** Relevant UV/vis (upper), RLS (middle) and fluorescence emission (lower) spectral features of  $\text{H}_2\text{TPPS}_4^{4-}$  porphyrin under different acidity conditions: (A)  $[\text{HCl}] = 0.01 \text{ M}$ ; (B)  $[\text{HCl}] = 2 \text{ M}$ ; (C)  $[\text{HCl}] = 12 \text{ M}$ ;  $[\text{porphyrin}] = 3 \times 10^{-6} \text{ M}$ ;  $T = 298 \text{ K}$ .

the hydrodynamic interactions with the solvent and on the interparticle interactions.

Under the condition  $kR \gg 1$ , the  $k^2$  dependence of the relaxation rate  $\Gamma$  loses validity, because of the sensitivity of light scattering to particle internal motions. If the diffusing objects are rigid and monodisperse, the  $k^2$  dependence and the Einstein–Stokes relation are still valid.<sup>41</sup> Moreover, fractal systems are generally anisotropic, so that the Einstein–Stokes relation underestimates the value of  $R_H$ . For slightly anisotropic fractal clusters, the following form is more suitable:<sup>49</sup>

$$\Gamma(k) = k^2 D \left( 1 + \frac{\alpha^2}{4\beta^2} \right) \quad (12)$$

where  $\beta = R_H/R_g$  is a measure of the porosity of a cluster and  $\alpha$  is directly related to its anisotropy.

## Results and Discussion

**Spectroscopic Characterization.** Even if the spectroscopic features of this porphyrin in aqueous solutions down to  $\text{pH} \sim 1$  have been already reported by various authors,<sup>8–12</sup> for the sake of comparison we will describe the most relevant changes under various acidity conditions.

At  $\text{pH} \sim 2$ , the diacid form  $\text{H}_4\text{TPPS}_4^{2-}$  is present (Figure 2, traces A), due to the protonation of the nitrogen atoms of the central macrocycle ( $\text{p}K_a = 4.9$ ).<sup>52</sup>

The UV/vis spectra show a Soret band at 434 nm, accompanied by two weaker Q-bands and the fluorescence emission at 668 nm with a weak longer wavelength shoulder. Under the present experimental conditions, the RLS spectra display a very weak intensity, with a well at 434 nm, due to photon loss and a low but detectable peak at 500 nm. This latter indicates that a low concentration of J-aggregated porphyrin is already formed. At  $[\text{HCl}] = 2 \text{ M}$  after equilibration, the narrow band at 490 nm, together with the red-shifted Q-bands at 636,

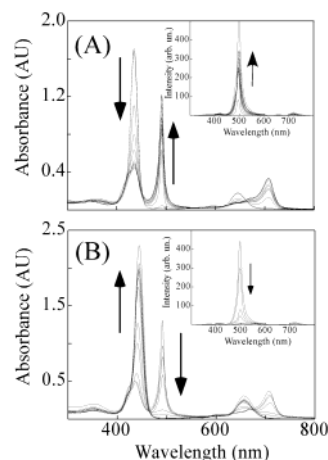


**Figure 3.** UV/vis spectral changes of a  $3 \times 10^{-6} \text{ M}$  aqueous solution of  $\text{H}_2\text{TPPS}_4^{4-}$  porphyrin on increasing HCl concentration: (A)  $[\text{HCl}] = 0.1\text{--}2 \text{ M}$ ; (B)  $[\text{HCl}] = 2\text{--}12 \text{ M}$ ;  $T = 298 \text{ K}$ . The insets show the corresponding RLS spectra.

668, and 708 nm in the UV/vis absorption spectra confirms the formation of J-aggregates (Figure 2, trace B).

Correspondingly, the fluorescence emission is substantially quenched, while the RLS spectra evidence a well-defined and intense peak at 500 nm and two smaller ones at 420 and 720 nm. In concentrated hydrochloric acid ( $[\text{HCl}] = 12 \text{ M}$ ), the UV/vis spectra show the formation of a new species having an intense Soret band at 444 nm and two weaker bathochromically shifted Q-band at 600 and 656 nm (Figure 2, trace C). The fluorescence spectra evidence a red shifted emission feature with a main band centered at 680 nm and a shoulder at about 705 nm. The monomeric nature of this species is supported by the very low intensity of the RLS profile which is very close to the neat solvent and is strongly modulated by the absorption of the sample. All these experimental findings suggest that this species is the fully protonated dicationic  $\text{H}_8\text{TPPS}_4^{2+}$  porphyrin.

Titration experiments have been carried out increasing the concentration of HCl up to 12 M, and they point out that acid-induced J-aggregates start to form at  $[\text{HCl}] \sim 0.1 \text{ M}$  and disappear for  $[\text{HCl}] > 6 \text{ M}$ . Figure 3 shows the UV/vis and RLS spectral changes upon the gradual conversion of the diacid form into the J-aggregated porphyrin (A) and the subsequent conversion of the J-aggregates into the fully protonated species, which is the only one present for  $[\text{HCl}] > 8 \text{ M}$  (B).

The absorbance values at 490 and 440 nm, together with the RLS intensity at the maximum (500 nm) and the fluorescence emission at 680 nm have been reported as a function of HCl concentration (Figure 4). Both these two latter quantities display a bell shaped profile with a maximum/minimum at about  $[\text{HCl}] = 2 \text{ M}$ . The UV/vis profile is similar for the absorbance at 490 nm (J band), even if the maximum is located at about  $[\text{HCl}] = 1 \text{ M}$ . Indeed, an inspection of the sigmoidal curve relative to the Soret band of the  $\text{H}_8\text{TPPS}_4^{2+}$  porphyrin (444 nm) reveals that this species begins to form appreciably for  $[\text{HCl}] > 2 \text{ M}$ .

The apparent discrepancy could be explained by the occurrence of resonant light scattering in the UV/vis experiments, which make the absorption at 490 nm not proportional to the concentration of the J-aggregated species. The RLS effect arises from an enhancement of the scattered light intensity in the red-edge portion of an absorption band. The occurrence of this phenomenon is related to a strong electronic coupling between adjacent chromophores, to the size and the geometry of the resulting aggregate and to intense molar absorbance of the monomeric constituents.<sup>14,38</sup> A consequence of resonance



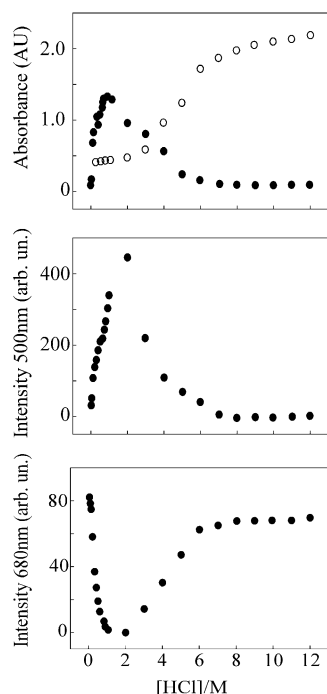


**Figure 4.** Plots of the various spectral parameters vs [HCl]: (upper plot) absorbance values at 440 (open circles) and 490 nm (full circles); (middle plot) RLS intensity at 500 nm; (lower plot) fluorescence emission intensity at 680 nm ( $\lambda_{\text{exc}} = 434$  nm).

enhanced light scattering in our system is that the band at 490 nm, as measured by a conventional spectrophotometer, is the sum of two extinction components due to absorption and scattering, respectively. This latter component determines a broadening of the band and the appearance of low intensity tail at the red edge of the J-band.<sup>53</sup>

**Light-Scattering Structural Investigations.** Previous light-scattering experiments on J-aggregates formed by lowering pH in unstirred solutions of  $\text{H}_4\text{TPPS}_4^{2-}$  revealed the presence of extended and weak networks, which exhibit fractal behavior. These experiments pointed out the different ability of protons or sodium cations in driving the final mesoscopic structure of the resulting clusters.<sup>16</sup> To get better insight into the structure of these porphyrin aggregates, we carried out both SLS and QELS measurements under different experimental conditions.

For porphyrin samples containing  $[\text{HCl}] < 0.01$  M, light-scattering experiments do not reveal any detectable amount of aggregates because of the strong electrostatic repulsion between the double negatively charged diacid species, which is not overcome by the modest ionic strength of the medium. Under these conditions, the kinetic barrier for the approach of monomers is very high and the probability of aggregation is very low.

On increasing the acid concentration ( $0.1 \text{ M} < [\text{HCl}] < 4$  M), QELS experiments revealed the presence of large aggregates, whose hydrodynamic radii increase from about 1000 Å up to about a micrometer, as shown in Figure 5. The decay rate of the autocorrelation functions,  $\Gamma$ , was measured at different  $k$  values. Its  $k^2$  dependence allowed us to extract the diffusion coefficient values at different acidic concentration and suggested that, although the large size of the aggregates, their internal rigidity is large and their intrinsic polydispersity is small enough to maintain the  $k^2$  dependence still valid. In this range of concentration, the protons are effective in screening the negative charge of the  $\text{SO}_3^-$  groups, actually lowering the screening Debye length and favoring the aggregation. This

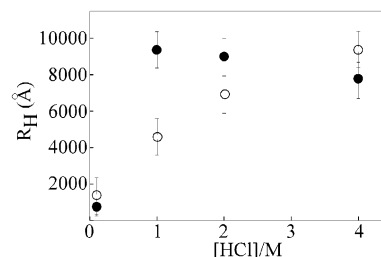


**Figure 5.** Measured hydrodynamic radii  $R_H$  from QELS experiments on samples containing J-aggregates at different HCl concentrations and using PF (open circles) and PL (full circles) mixing orders ( $[\text{porphyrin}] = 3 \times 10^{-6}$  M;  $T = 298$  K).

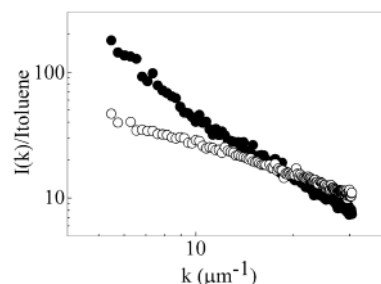


**Figure 6.** SLS normalized intensity profiles  $I(k)$  vs  $k$  for aggregated  $\text{H}_4\text{TPPS}_4^{2-}$  in the regime of complete aggregation, using PF (open circles) and PL (full circles) mixing orders ( $[\text{HCl}] = 0.1$  M;  $[\text{porphyrin}] = 3 \times 10^{-6}$  M;  $T = 298$  K).

phenomenon is driven by the interparticle potential which can be described through the well-known Derjaguin–Landau–Verwey–Overbeek potential (DLVO),<sup>54–56</sup> which is related to the presence of a diffuse double layer surrounding colloidal particles.

The smaller size measured for the porphyrin aggregates at  $[\text{HCl}] = 0.1$  M can be explained by considering that the interaction between diacid porphyrins is still repulsive (charge 2 $-$ ) with a long screening length and the weak attractive van der Waals forces ( $\propto r^{-6}$ ) are scarcely effective, leading to a small probability of interaction. However, after an induction period due to this small sticking probability, the DLVO potential, whose attractive component depends on the third inverse power of the interparticle distance, favors the adhesion between small clusters ( $\lambda > \nu$ ). As shown in Figure 6 (closed circles), the scattered intensity vs  $k$  follows a power law with a fractal dimension equal to  $1.75 \pm 0.05$  (in the present case the aggregate size fulfills the conditions  $kR \gg 1$  and  $R/L > 50$ ), indicating that small clusters are able to self-interact leading to larger aggregates with a DLCCA mechanism. For  $[\text{HCl}] \geq 2$  M, the net charge of the molecules is small enough to lower the screening length and to give rise to a larger extent of aggregation as indicated by the values of the hydrodynamic radii in Figure 5. Under these conditions, the sticking probability between monomers is finite. After an early RLA stage, which leads to the formation of typical sized aggregates (nuclei), these latter trigger a diffusion-limited aggregation process depleting the solution from monomers ( $\lambda < \nu$ ). The crossover between aggregation mechanisms during the kinetic growth has already been reported in the salt-induced fractal aggregation of the dicationic *trans*- $\text{H}_2\text{P}_{\text{agg}}$ .<sup>32</sup>

Figure 7 shows the scattered intensity profile obtained by a combination of SLS data, at wide and small angles, on an aggregated sample at  $[\text{HCl}] = 2$  M (PL mixing). The scattered intensity vs  $k$  follows a power law with a fractal exponent suggesting a DLA mechanism ( $d_f = 2.5 \pm 0.03$ ). At lower  $k$  values, where the curvature of the intensity profile appears, the Guinier region begins. A reliable evaluation of the radius of

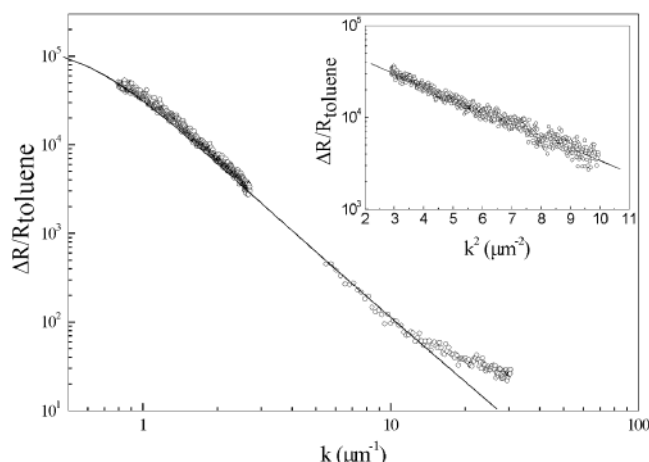


**Figure 7.** SLS and SALS normalized intensity profiles  $I(k)$  vs  $k$  for aggregated  $H_4TPPS_4^{2-}$  in the regime of complete aggregation, using PL mixing order ( $[HCl] = 2$  M;  $[porphyrin] = 3 \times 10^{-6}$  M;  $T = 298$  K). The continuous line is the fit according to eq 6. The inset reports the normalized intensity profiles  $I(k)$  vs  $k^2$  (the continuous line represents the Guinier fit) for aggregated  $H_4TPPS_4^{2-}$  in the regime of complete aggregation, using PF mixing order.

gyration of the clusters would require more data point at  $k < 1 \mu m^{-1}$ . However, the clear knee in the profile allows for estimating that the clusters are certainly larger than  $1 \mu m$ . At higher  $k$  values, the intensity profile changes again toward a Guinier behavior, giving the size of the seeds which triggered the aggregation,  $R_0 \cong 600$  Å.

At  $[HCl] = 4$  M, the net charge on the monomer becomes very small and the ionic strength is large enough to almost reduce to zero the screening length. The aggregation process is driven almost entirely by attractive forces and it takes place by nucleation, without any fractal arrangement. Any further increase of the acid concentration leads to the full protonation of the sulfonate end groups and to the disruption of the aggregates. Because of the presence of the two positive charges, the  $H_8TPPS_4^{2+}$  porphyrin does not self-interact even under these extreme ionic strength conditions, as evidenced by SLS, QELS, and RLS experiments.

**Influence of the Mixing Order.** Previous reports on porphyrin aggregation have pointed out the necessity of setting up a protocol to mix the reagents in order to get reproducible results.<sup>15,57,58</sup> This issue becomes particularly relevant when dealing with kinetic studies. Pasternack et al. suggested the importance of the mixing order in studying the kinetic of supramolecular assembling of the *trans*- $H_2P_{agg}$  porphyrin onto the surface of DNA<sup>57</sup> and the formation of J-aggregates from  $H_2TPPS_4^{4-}$ .<sup>58</sup> In our hands, aggregation experiments with  $H_2TPPS_4^{4-}$ , performed using  $[HCl] = 0.1$  M and  $[porphyrin] = 5 \times 10^{-6}$  M (data not shown), gave reproducible kinetic traces, exhibiting a sigmoidal behavior with a characteristic induction period, when the porphyrin stock solution was added as last reagent (PL). On the contrary, the reverse mixing (PF) gave very different kinetic traces and in some instance aggregation did not occur even after days.

In colloidal systems, as in the present case, the kinetics of growth and the relative mechanism drive the morphology of the resulting aggregate. Therefore, the mixing order of the reagents turns out as a relevant factor to be controlled. Indeed, the SLS data reported in Figure 6 evidence that the final aggregates exhibit a fractal structure when the porphyrin is added in an acidic environment (PL mixing), while they form statistical isotropic objects using the PF mixing, as proved by the Ornstein-Zernike behavior of the scattered intensity profile.

As previously described, Figure 7 reports the SLS data, at wide and small angles, for an aggregated sample at  $[HCl] = 2$  M, which point out the presence of a DLA fractal structure for the PL mixing. The insert shows the Guinier type plot of the SALS profile corresponding to a sample obtained under the same experimental conditions except by a PF mixing. In this case, the gyration radius of the aggregates is  $R_g = 1 \mu m$  and there is no fractal arrangement in the whole investigated  $k$  range. Even in this case, above  $10 \mu m^{-1}$ , we can estimate the seed size of about 600 Å.

The different observations and the apparent low reproducibility can be ascribed to the fact that (i) the addition of concentrated acid to a diluted porphyrin aqueous solution (PF mixing) produces a proton concentration gradient and the consequential formation of statistical isotropic objects whose number and size are not reproducible and that (ii) the SLS technique is averaging on the observation volume in which there is a spatial distribution of DLA and DLCCA clusters. This effect becomes very important when the final concentration of acid is not high (e.g.,  $[HCl] = 0.1$  M) and is mainly due to the large volumetric ratio between the reagent solutions to be mixed. The color of the porphyrin solution allows for an easy visualization of this phenomenon. When a small volume of a stock porphyrin solution is added to an aqueous HCl solution ( $[HCl] = 0.1$  M), it remains clearly evident and localized as soon as after injection, and it does not mix even after a prolonged time. On the contrary, when the required amount of HCl is added to a diluted porphyrin solution, the acid starts to flow quite soon as evidenced by the green color due to the formation of the diacid form throughout the solution.

On these bases, the relative concentrations of the stock solution of both reagents play an important role, as well as the lag time between injecting a reagent and mixing the solution. All these parameters, together with aging and history of the samples,<sup>34</sup> should be taken into account for a correct interpretation of the kinetic and structural parameters of such supramolecular systems.

## Conclusions

Our results indicate that, upon the addition of hydrochloric acid, the diacid  $H_2TPPS_4^{2-}$  porphyrin begins to form J-aggregates at about pH 1. These species are stable under acidic conditions up to 4 M HCl. The subsequent protonation of the sulfonate end groups leads to a disruption of the hydrogen-bonding network and the electrostatic interaction with the protonated and positively charged nitrogen atoms of the core, responsible for the edge-to-edge arrangement of adjacent porphyrins. In concentrated HCl, only the fully protonated dicationic porphyrin is present in a monomeric form. A combination of light-scattering techniques have evidenced the occurrence of structural rearrangements of the clusters depending on the HCl concentration. These effects are related to the DLVO potential which controls the interactions between particles during the aggregation of colloidal systems. Both the parallel reduction of the net charge on the porphyrin and the increase of the ionic strength on increasing the acid concentration drive the system to a statistical nucleating aggregate passing through a DLCCA and a DLA aggregation regime.

In such complex systems, the experimental protocol to mix the reagents is an important parameter which can strongly affect the kinetics of growth of the clusters and their final mesoscopic structure.

**Acknowledgment.** The authors thank the Ministero dell'Istruzione, dell'Università e della Ricerca Scientifica (MIUR), Programmi

di Ricerca Scientifica di Rilevante Interesse Nazionale, Cofinanziamento 2002–2003, and the CNR for financial support.

## References and Notes

- (1) Lehn, J. M. *Supramolecular Chemistry*, VCH: Weinheim, Germany, 1995.
- (2) Spano, F. C.; Mukamel, S. *Phys. Rev. A* **1989**, *40*, 5783.
- (3) Mobius, D. *Acc. Chem. Res.* **1981**, *14*, 63.
- (4) Nakahara, H.; Fukuda, K.; Mobius, D.; Kuhn, H. *J. Phys. Chem.* **1986**, *90*, 6144.
- (5) Daehne, S. *Photogr. Sci. Eng.* **1979**, *23*, 219.
- (6) Fidder, H.; Terpstra, J.; Wiersma, D. A. *J. Chem. Phys.* **1991**, *94*, 6895.
- (7) Moll, J.; Daehne, S.; Durrant, J. R.; Wiersma, D. A. *J. Chem. Phys.* **1995**, *102*, 6362.
- (8) Ohno, O.; Kaizu, Y.; Kobayashi, H. *J. Chem. Phys.* **1993**, *99*, 4128.
- (9) Ribò, J. M.; Crusats, J.; Farrera, J. A.; Valero M. L. *J. Chem. Soc., Chem. Commun.* **1994**, 681.
- (10) Akins, D. L.; Zhu, H. R.; Guo, C. *J. Phys. Chem.* **1994**, *98*, 3612.
- (11) Pasternack, R. F.; Schaefer, K. F.; Hambright, P. *Inorg. Chem.* **1994**, *33*, 2062.
- (12) Maiti, N. C.; Ravikanth, M.; Mazumdar, S.; Periasamy, N. *J. Phys. Chem.* **1995**, *99*, 17192.
- (13) Rubires, R.; Crusats, J.; El-Hachemi, Z.; Jaramillo, T.; Lopez, M.; Valls, E.; Farrera, J. A.; Ribò, J. M. *New J. Chem.* **1999**, 189.
- (14) Parkash, J.; Robblee, J. H.; Agnew, J.; Gibbs, E.; Collings, P.; Pasternack, R. F.; de Paula, J. C. *Biophys. J.* **1998**, *74*, 2089.
- (15) Collings, P. J.; Gibbs, E. J.; Starr, T. E.; Vafeek, O.; Yee, C.; Pomerance, L. A.; Pasternack, R. F. *J. Phys. Chem. B* **1999**, *103*, 8474.
- (16) Micali, N.; Mallamace, F.; Romeo, A.; Purrello, R.; Monsù Scolaro, L. *J. Phys. Chem. B* **2000**, *104*, 5897.
- (17) Ribò, J. M.; Rubires, R.; El-Hachemi, Z.; Farrera, J. A.; Campos, L.; Pakhomov, G. L.; Vendrell, M. *Mater. Sci. Eng. C* **2000**, *11*, 107.
- (18) Maiti, N. C.; Mazumdar, S.; Periasamy, N. *J. Phys. Chem. B* **1998**, *102*, 1528.
- (19) Lauceri, R.; Gurrieri, S.; Bellacchio, E.; Contino, A.; Monsù Scolaro, L.; Romeo, A.; Toscano, A.; Purrello, R. *Supramol. Chem.* **2000**, *12*, 193.
- (20) Micali, N.; Romeo, A.; Lauceri, R.; Purrello, R.; Mallamace, F.; Monsù Scolaro, L. *J. Phys. Chem. B* **2000**, *104*, 9416.
- (21) McRae, E. G.; Kasha, M. In *Physical Processes in Radiation Biology*; Augenstein, L.; Mason, R.; Rosenberg, B., Eds.; Academic Press: New York, 1964; pp 23–42.
- (22) Knapp, E. W. *Chem. Phys.* **1984**, *85*, 73.
- (23) Hunter, C. A.; Sanders, M. K. *J. Am. Chem. Soc.* **1990**, *112*, 5525.
- (24) Kano, K.; Minamizono, H.; Kitae, T.; Negi, S. *J. Phys. Chem.* **1997**, *101*, 6118.
- (25) Kano, K.; Fukuda, K.; Wakami, H.; Nishiyabu, R.; Pasternack, R. F. *J. Am. Chem. Soc.* **2000**, *122*, 7494.
- (26) Vicsek, T. *Fractal Growth Phenomena*; World Scientific: London, 1992.
- (27) Leyvraz, F. In *On Growth and Form*; Stanley, H. E., Ostrowsky, N., Eds.; Martinus Nijhoff Publisher: Dordrecht: The Netherlands, 1986; p 136.
- (28) Meakin, P.; Vicsek, T.; Family, F. *Phys. Rev. B* **1985**, *31*, 564.
- (29) Mallamace, F.; Micali, N.; Trusso, S.; Monsù Scolaro, L.; Romeo, A.; Terracina, A.; Pasternack, R. F. *Phys. Rev. Lett.* **1996**, *76*, 4741.
- (30) Micali, N.; Monsù Scolaro, L.; Romeo, A.; Mallamace, F. *Phys. Rev. E* **1998**, *57*, 5766.
- (31) Monsù Scolaro, L.; Romeo, A.; Mallamace, F.; Micali, N.; Purrello, R. *Nuovo Cimento D* **1998**, *20*, 2207.
- (32) Mallamace, F.; Monsù Scolaro, L.; Romeo, A.; Micali, N. *Phys. Rev. Lett.* **1999**, *59*, 3480.
- (33) Mallamace, F.; Micali, N.; Romeo, A.; Monsù Scolaro, L. *Curr. Opin. Colloid Interface Sci.* **2000**, *5*, 49.
- (34) Monsù Scolaro, L.; Castriciano, M. A.; Romeo, A.; Mazzaglia, A.; Mallamace, F.; Micali, N. *Physica A* **2002**, *304*, 158.
- (35) Ribò, J. M.; Crusats, J.; Saguès, F.; Claret, J.; Rubires, R. *Science* **2001**, *292*, 2063.
- (36) Rubires, R.; Farrera, J.-A.; Ribò, J. M. *Chem.—Eur. J.* **2001**, *7*, 436.
- (37) Buchler, J. W.; Kuenzel, F. M.; Mayer, U.; Nawra, M. *Fresen. J. Anal. Chem.* **1994**, *348*, 371.
- (38) Pasternack, R. F.; Collings, P. J. *Science* **1995**, *269*, 935.
- (39) Pasternack, R. F.; Bustamante, C.; Collings, P. J.; Giannetto, A.; Gibbs, E. J. *J. Am. Chem. Soc.* **1993**, *115*, 5393.
- (40) Mallamace, F.; Micali, N.; Trusso, S.; Chen, S. H. *Phys. Rev. E* **1995**, *51*, 5818.
- (41) Berne, B. J.; Pecora, R. *Dynamic Light Scattering with Application to Chemistry, Biology and Physics*; J. Wiley and Sons: New York, 1976.
- (42) Ornstein, L. S.; Zernike, F. *Proc. Akad. Sci.* **1914**, *17*, 793.
- (43) Stanley, H. E.; Ostrowsky, N. *On Growth and Form*; NATO ASI Series; Martinus Nijhoff Publishers: Dordrecht, The Netherlands, 1986.
- (44) Mallamace, F.; Micali, N. *Riv. Nuovo Cimento* **1992**, *15*, 1.
- (45) Kolb, M.; Herrmann, H. *J. Phys. Rev. Lett.* **1987**, *59*, 454.
- (46) Keefer, K. D.; Schaefer, D. W. *Phys. Rev. Lett.* **1986**, *56*, 2376.
- (47) Chen, S. H.; Teixeira, J. *Phys. Rev. Lett.* **1986**, *57*, 2583.
- (48) Cummins, H. Z. In *Photon Correlation and Light Beating Spectroscopy*; Cummins, H. Z., Pike, E. R., Eds.; Plenum Press: New York, 1974.
- (49) Schaefer, D. W.; Han, C. C. In *Dynamic Light Scattering*; Pecora, R., Ed.; Plenum: New York, 1985.
- (50) Martin, J. E.; Schaefer, D. W. *Phys. Rev. Lett.* **1984**, *53*, 2457.
- (51) Lindsay, H. M.; Klein, R.; Weitz, D. A.; Lin, M. Y.; Meakin, P. *Phys. Rev. A* **1989**, *39*, 3112.
- (52) Kalyanasundaram, K. *Photochemistry of Polypyridine and Porphyrin Complexes*; Academic Press: London, 1992; p 428.
- (53) Micali, N.; Mallamace, F.; Castriciano, M. A.; Romeo, A.; Monsù Scolaro, L. *Anal. Chem.* **2001**, *73*, 4958.
- (54) Verwey, E. J.; Overbeek, J. Th. G. *Theory of the Stability of Lyophobic Colloids*; Elsevier, Amsterdam, 1984.
- (55) Derjaguin, B. V.; Landau, L. *Acta Phys. Chim. Debricina* **1941**, *14*, 633.
- (56) Ottewill, R. H. *Spec. Rep. Chem. Soc. Colloid Sci.* **1973**, *1*, 175.
- (57) Pasternack, R. F.; Gibbs, E. J.; Collings, P. J.; de Paula, J. C.; Turzo, L. C.; Terracina, A. *J. Am. Chem. Soc.* **1998**, *120*, 5873.
- (58) Pasternack, R. F.; Fleming, C.; Herring, S.; Collings, P. J.; de Paula, J. C.; DeCastro, G.; Gibbs, E. J. *Biophys. J.* **2000**, *79*, 550.